Study of strontium doped $Nd_2FeO_{4+\delta}$ cathode material for intermediate temperature solid oxide fuel cells application

Study of strontium doped $Nd_2FeO_{4+\delta}$ cathode material for intermediate temperature solid oxide fuel cells application

J D Punde[1] and V N Chaudhari[2]

[1] Department of Physics, S S Girls' College, Gondia-441 601, India.
[2] Department of Physics, RTM Nagpur University, Nagpur-440 033, India.

email: vj1784@gmail.com

Abstract. The series of $Nd_{2-x}Sr_xFeO_{4+\delta}$ ($x = 0.1$ - 0.4) single phase compound is prepared with crystallite size in submicron range using combustion synthesis technique. The agglomeration of the submicron sized crystallites resulted into formation of porous electrode layer is realized from scanning electron microscopy. The dc conductivity results showed maximum σ for $x = 0.2$, which also exhibited minimum activation energy. The comparative low dc conductivity with literature reports is due to high porosity as obtained from agglomerated submicron crystallites. Variation in conductivity in $Nd_{2-x}Sr_xFeO_{4+\delta}$ is Sr-dependent and understood from defect chemistry. The complex impedance plots of the symmetric cell showed decrease in the real axis intercept with increased temperature in turn reduced area specific resistance (ASR). $Nd_{1.8}Sr_{0.2}FeO_{4+\delta}$ cathode exhibits lowest ASR (= 1.92±0.015 Ohm cm^2) at 973 K. The oxygen partial pressure dependent ASR indicated that the charge transfer at electrode-electrolyte interface is the rate limiting factor while oxygen reduction reaction (ORR).

Keywords. IT-SOFC, dc conductivity, $Nd_{2-x}Sr_xFeO_{4+\delta}$ cathode materials, symmetric cell, EIS study.

1. Introduction

In recent past, extensive studies were carried out on layered perovskite oxides with K_2NiF_4-type structure due to their number of expedient properties [1,2]. Among the mixed conducting oxides, the Ruddlesden-Popper phases $Ln_2NiO_{4+\delta}$ have received much attention in last two decades [3]. The A_2BO_4 (rare earth/alkaline earth element as A-site cations and transition metal on the B-site) layered perovskites are deeply viewed as promising cathode adhering to their astonishing environmental stability and versatile applications. The doped alkaline earth elements, because of their advanced mixed ionic and electronic conductivities has been alternative choices for cathode materials in intermediate temperature solid oxide fell cells (IT-SOFC) [4-7]. The K_2NiF_4-type manganates, nickelates, cuprates and ferrates are more thermally and chemically stable as compare to the corresponding perovskite -type oxides [8].

Previously, several $Ln_2NiO_{4+\delta}$-based materials, (Ln = La, Pr, Nd, or Sm) have been the well-liked choices as cathode materials for IT-SOFC [9-14]. Huang et al. in his studies on $LaSrNiO_{4+\delta}$ showed that the electrode and SDC electrolyte forms close contact with each other. He obtained the ASR of 3.90-ohm cm^2 at 973 K [15]. According to literature, increasing Sr concentration improves p-type electrical conductivity in La_2NiO_4 [16]. As per literature, oxygen partial pressure and preparation temperature has remarkable impact on producing dissimilar defects in K_2NiF_4-type structure [17-19]. Similar properties are exhibited by the materials like $Ln_2FeO_{4+\delta}$ (Ln = La, Ba). Improved cathodic properties with Sr concentration are reported by Jin et al. [20]. They successfully obtained K_2NiF_4-type structures for $Ba_{2-x}Sr_xFeO_{4+\delta}$ in the range $0.5 \leq x \leq 1.0$. Guo et al. prepared $Nd_{2-x}Sr_xFeO_{4+\delta}$ (x = 0.5-1.0) by glycine-nitrate method and reported lowest ASR of 2.75 ohm cm^2 at 973 K for $x = 1.0$ with $Sm_{0.2}Gd_{0.8}O_{1.9}$ (SDC) based electrolyte [21]. A comprehensive literature survey suggests that, the $Nd_{2-x}Sr_xFeO_{4+\delta}$ have been given less attention as cathode materials and there is an adequate scope still

available for preparing superfine polycrystalline $Nd_{2-x}Sr_xFeO_{4+\delta}$ through alternative techniques to achieve better electrical and electrochemical properties for IT-SOFC applications.

In the light of aforesaid facts, current studies are undertaken with the goal of synthesis and research of $Nd_{2-x}Sr_xFeO_{4+\delta}$ (x = 0.1-0.4) cathode materials using combustion technique (self-assisted/without fuel) for IT-SOFC applications. The sample investigations include a variety of measurements using X-ray powder diffraction, scanning electron microscopy, four-probe dc conductivity. Temperature and oxygen partial pressure based electrochemical impedance spectroscopic (EIS) studies were carried out supported on $Ce_{0.9}Gd_{0.1}O_{1.95}$ (GDC) electrolyte with Cathode/GDC/Cathode (symmetric cell) configuration.

2. Experimental

The $Nd_{2-x}Sr_xFeO_{4+\delta}$ (x = 0.1-0.4) powdered compositions were prepared by following combustion synthesis method [14]. Briefly, Nd, Sr and Fe acetates (Sigma Aldrich, 99.9% pure) were taken as initial reagents and dehydrated at 393 K for 6 h in order to eradicate the traces of existing humidity. All of the required reagents measured in their stoichiometric fraction were dissolved in the doubly deionised distilled water. The liquid suspensions were then combined together in one beaker to homogenize and heated at 373 K using rota-mantle subjecting to constant stirring till complete water evaporation. The obtained residue was then burned in an electric muffle furnace at around 523 K. The ground powder then uniaxially compressed at 2.94 N m^{-2} pressure using Specac stainless steel die-punch and hydraulic press (UK) to obtain pellets of 9 mm diameter and 2 mm thickness. The prepared pellets were fired lastly at 1273 K for 10 h. The $Nd_{2-x}Sr_xFeO_{4+\delta}$ when x = 0.1, 0.2, 0.3 and 0.4 are hereafter designated as NSFO-0.1, NSFO-0.2, NSFO-0.3 and NSFO-0.4, respectively.

Electrical conductivity (d.c.) measurements were done on sintered pellet, dc sputtered on both the flat surfaces resulting in good ohmic contact using four probe dc conductivity method [14,22] in the temperature range 773-973 K. Before conductivity measurement, the sintered pellets were griped in a cell holder and heated at 973 K for 1 h so that the charge carriers should get homogenize. The resistivity measurement with temperature variation is done using four-probe dc conductivity method with the help of Keithley 6221 current source in association with 2182A nanovoltmeter used in delta mode. The accuracy of ±1 °C was managed with the help of Eurotherm 2216e temperature controller during the entire measurements.

X-ray powder diffraction (XRPD) characterizations on the prepared samples were performed using PANalytical X'pert PRO (Philips) using CuK_α radiations. The crystallographic measurements 2θ versus peak intensity were ranging from 10° to 100° with the step size of 0.025° and time/step of 5 s, with the help of Pixel 1D detector. The crystallite size based on Debye-Scherer formula was calculated using software for all the compositions under study as explained elsewhere [22]. The morphological and compositional studies of the cathode on symmetric cells were done using scanning electron microscope (FEG-SEM) with EDS attachment. The sintered density of the entire samples was measured as derived from Archimedes' principle [14]. Hardness measurements were performed using the Vickers indentation technique [14,31].

The slurry/ink of optimized cathode (based on dc conductivity measurements) was prepared with 1 gram of $Nd_{1.8}Sr_{0.2}FeO_{4+\delta}$ powder, PVB binder, sodium-free corn oil suspended in ethyl methyl ketone and ball milled at 100 rpm for 2 h using planetary monomill (Fritsch Pulverisette-6, Germany). The 10 mol% GDC nano-powder acquired from Aldrich chemicals, pressed as described above to prepare pallets of 10mm ×1mm diameter and thickness. Afterwards, the pellets were ignited at 1673 K for 6 h to obtain solid GDC pellets with sintered density of 96%. A layer of prepared slurry/ink of cathode is applied on both plain faces of GDC pellet using a spin coater to obtain symmetric cells of $Nd_{1.8}Sr_{0.2}FeO_{4+\delta}$/GDC/ $Nd_{1.8}Sr_{0.2}FeO_{4+\delta}$ configuration henceforth called as Cell-0.2.

For EIS measurements, Auto-programmed Solartron 1255B frequency response analyser along with a Solartron SI 1287 electrochemical interface is used in the frequency range from 1mH to 1MH,

and at reduced oxygen atmosphere of 0.1% to 21% as explained in another paper [22]. An ac signal of 50 mV was applied.

3. Results and discussion

3.1 Phase and structural analysis using XRD

Typical X-ray powder diffraction (XRPD) spikes of $Nd_{2-x}Sr_xFeO_{4+\delta}$ (x = 0.1, 0.2, 0.3 and 0.4) are shown in Fig. 1(a)-(d), respectively. The diffraction pattern appears broader than typically observed for any good crystalline solids. This superfine crystalline nature of materials attributes to broadened diffracted lines. Fig. 1(a) reveals characteristics diffraction peaks (experimental) are strongly matching with tetragonal $Nd_{2-x}Sr_xFeO_{4+\delta}$ of JCPDS file No. 01-076-1876. Similar results were obtained for the compositions when x = 0.2-0.4. Nonexistence of spike(s) due to primary reagent validates the formation of single-phase compounds with K_2NiF_4 structure. The reactivity of NSFO with GDC electrolyte was studied further. The XRPD pattern (not shown here) of a cathode and GDC blend in a weight ratio of 1:1 do not show any new peaks even after heating at 1,473 K for 24 h. This ensures that, there is no chemical reaction between them which confirms brilliant chemical compatibility between $Nd_{2-x}Sr_xFeO_{4+\delta}$ cathode materials and GDC electrolyte.

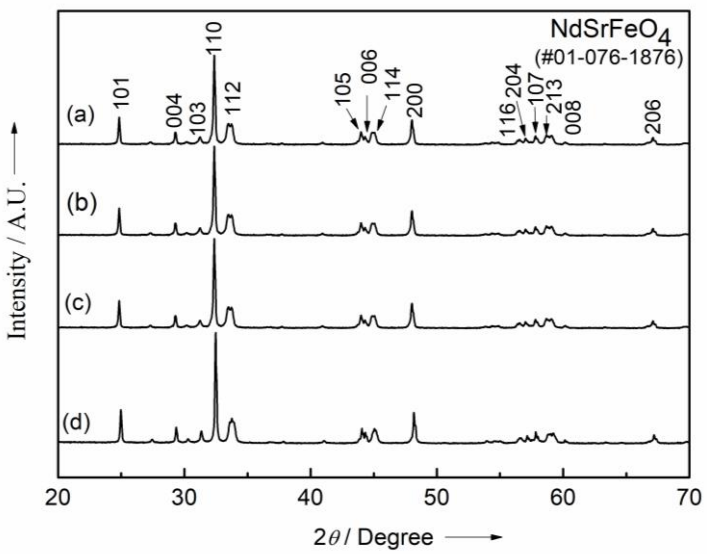

Figure 1. X-ray powder diffraction patterns of $Nd_{2-x}Sr_xFeO_{4+\delta}$ when (a) x = 0.1, (b) x = 0.2, (c) x = 0.3 and (d) x = 0.4

Table 1 exhibits comparison between the values of lattice cell constants evaluated for all solid solutions. A close analysis of Table 1 tells that lattice cell constant a change very minutely, in contrast, the figure c has increased appreciably with addition in Sr concentration within the solid solubility limit (x = 0.1 - 0.4). Parallel results are reported in literature [23,24] for non-varying number of a, while a slow increase in c with Sr concentration for K_2NiF_4-type materials. A systematic variation of c and v advocates single phase solid solutions are formed for the all the compositions of $Nd_{2-x}Sr_xFeO_{4+\delta}$. Moreover, table 1 illustrates nearly similar values of crystallite size (189-206 nm), sintered density (82-87%) and microhardness number (323-419 HV) for the entire series of $Nd_{2-x}Sr_xFeO_{4+\delta}$ compositions. Evidently, microstructure of solid solutions is not affected by dopant concentration. The experimental and theoretical values of at% of elements of $Nd_{1.8}Sr_{0.2}FeO_{4+\delta}$ as obtained from EDS and calculations respectively are given in Table 2. The figures are closely matching which confirms that, the stoichiometric compounds are formed.

Table 1. A comparison of tolerance factor (t), lattice cell constants (a, c and v), average crystallite size (C_s), % density (ρ) and micro hardness number (HV) of $Nd_{2-x}Sr_xFeO_{4+\delta}$ (x = 0.1 – 0.4).

x	t	a (nm)	c (nm)	v (nm^3)	C_s (nm)	ρ (%)	HV
0.1	0.939	0.376±0.004	1.317±0.006	0.1862±0.015	189.5±0.045	82.81±0.44	323±4
0.2	0.942	0.376±0.002	1.320±0.005	0.1866±0.018	197.9±0.051	85.28±0.57	350±3
0.3	0.944	0.376±0.007	1.322±0.008	0.1869±0.021	204.4±0.048	87.25±0.52	419±6
0.4	0.945	0.376±0.005	1.326±0.007	0.1875±0.022	206.2±0.065	84.56±0.48	412±9

3.2 Morphological studies using SEM

The SEM photographs of broken surface through the cathode–GDC interface of cell-0.2 are portrayed in Fig. 2. A close look at figure reveals that, there is agglomeration in submicron crystallites of the $Nd_{1.8}Sr_{0.2}FeO_{4+\delta}$ accounts for evenly distribution of grains all over the cathode (shown as an inset). Preset sintering temperature of 1273 K was chosen (with reference to our prior studies and literature reports) to obtain the best sintering performance. Figure shows, homogeneous contact throughout the interface of electrode and electrolyte is formed and no cracks or separation between them is observed despite several heating and cooling cycles of temperature. Further, the electrode forms highly porous structure is with an average thickness of 14.2 µm over GDC electrolyte which appears fully dense. The estimated elemental atomic percentage for experimental and theoretical values of $Nd_{1.8}Sr_{0.2}FeO_{4+\delta}$ is compared in Table 2 supporting the formation of stoichiometric compounds.

Table 2. A comparison of experimentally and theoretically estimated at% values for elements of $Nd_{1.8}Sr_{0.2}FeO_{4+\delta}$

Element	Concentration at %	
	Theoretical	Experimental
O	57.1429	57.79±0.9
Fe	14.2857	13.97±0.7
Sr	02.8571	02.74±0.3
Nd	25.7143	25.50±0.6
Total	100.000	100.00±0.4

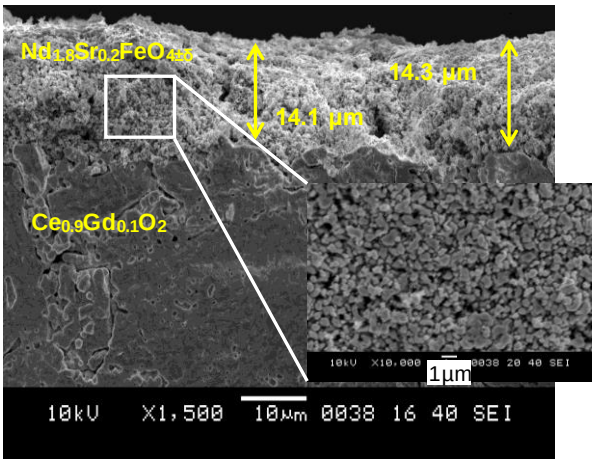

Figure 2. Scanning electron microphotograph of electrode-electrolyte interface of prepared cell (inset shows magnified image of porous cathode material)

3.3 dc conductivity using four probe method

The dc conductivity taking into account electronic contribution of MIEC cathode is measured using four-probe method. The deviation in d.c. conductivity for $Nd_{2-x}Sr_xFeO_{4+\delta}$ (x = 0.1, 0.2, 0.3 and 0.4) is shown in Fig. 3 as a parametric function of temperature. Whole sample follows Arrhenius law within

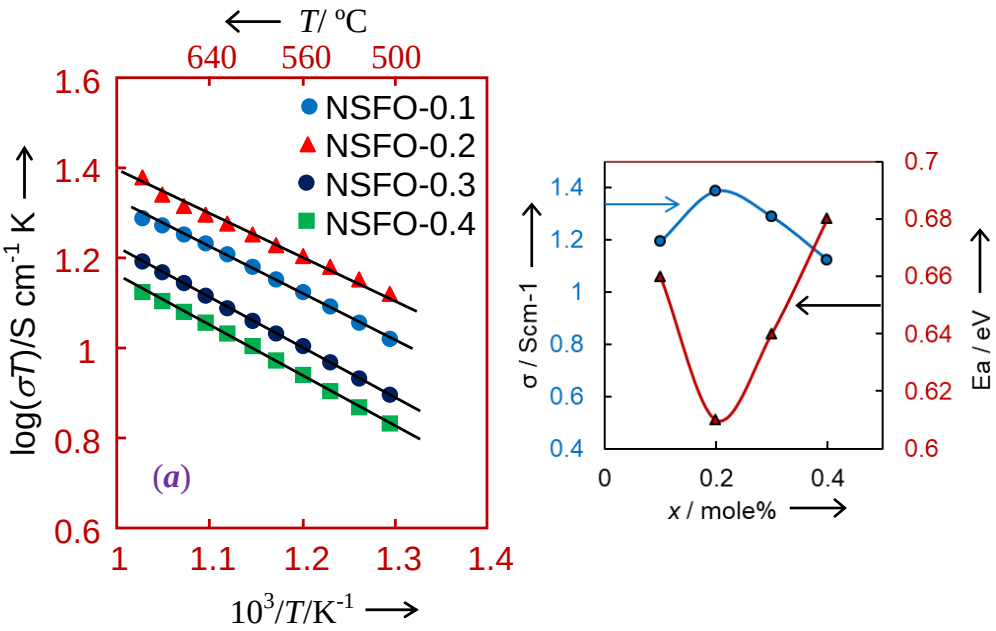

Figure 3. (a) Arrhenius plots for $Nd_{2-x}Sr_xFeO_{4\pm\delta}$ when x = 0.1 – 0.4; (b) Variation of σ with x at 973 K.

the entire measuring temperature range as follows,

$$\sigma T = (\sigma T)_0 \exp\left(\frac{-E_a}{kT}\right) \quad (1)$$

where $(\sigma T)_0$ is pre-exponential factor, k is Boltzmann constant, T is temperature and E_a is activation energy. It is clear from the figure that, conductivity firstly move above with raising Sr content in $Nd_{2-x}Sr_xFeO_{4+\delta}$ but then decreases after reaching a maximum at x = 0.2 (Fig. 3(b)). The obtained activation energies for NSFO-0.1, NSFO-0.2, NSFO-0.3 and NSFO-0.4 are 0.66, 0.66, 0.64 and 0.68 eV, respectively. It is evident from the figure that, the compositions with minimum activation energy are in close agreement with those having maximum conductivity. An extensive study of Table 1 reveals that, crystallite size of prepared material is within the range of 189-206 nm and the sintered density is roughly similar for all studied compositions. The behaviour in conductivity with respect to change in Sr content (Fig. 3(a)) is because of extrinsic defects formed as reported in literature [14, 26-31]. Again, it is advisable to notice here that, the electrical properties in $Ln_{2-x}Sr_xMO_4$ (M = Ni, Co, Fe, Mn) compounds are enhanced because of the charge disproportionation Fe^{3+}/Fe^{5+} according to Mössbauer spectroscopy [25]. At present, conductivity data corresponding to current system is unavailable in the literature to make any comparison. Since $Nd_{1.8}Sr_{0.2}FeO_{4+\delta}$ exhibited highest d.c. conductivity (σ_{max} = 49 S cm^{-1} at 913 K) compared to the other studied compositions, so, it was considered for electrochemical studies.

3.4 Electrochemical performance using EIS

The value of ASR gives important information about the kinetics in the oxygen reduction reaction (ORR) on the cathode surface. The complex impedance spectroscopic (CIS) plot for Cell-0.2 at different temperatures is shown in Fig. 4 as a representative of all. The measurements are taken over the frequency range from 1mH (low frequency) to 1MH (high frequency). Figure shows depressed semi-circular arcs in the region of small frequency whereas at above frequency semicircular arc is absent due to constraint of allocated frequency ($\leq$ 1 MHz). The intercept (high frequency) at real axis (R_{GDC}), belongs to GDC electrolyte and small frequency region semicircular arc is accredited to the sample electrode. The ever-increasing semicircular arcs intercepting at real axis with decrease in temperature signify an increase in resistance of GDC electrolyte (R_{GDC}) and also the ASR of electrode. The area specific resistance as a function of temperature for Cell-0.2 is shown (as an inset) in Fig. 4 for the $Nd_{2-x}Sr_xFeO_{4+\delta}$ cathodes. The Arrhenius plots are obtained taking log(ASR) on the ordinate axis and 1000/T on the abscissa. The activation energy as determined from the slope is found to be 1.0 eV for NSFO electrodes. It was seen that, initially, the ASR decreases with the addition of Sr concentration but then increases on further addition of Sr concentration. The composition $Nd_{1.8}Sr_{0.2}FeO_4$ shows lowest area specific resistance ($\simeq$1.92 ohm cm^2) at 973 K in air.

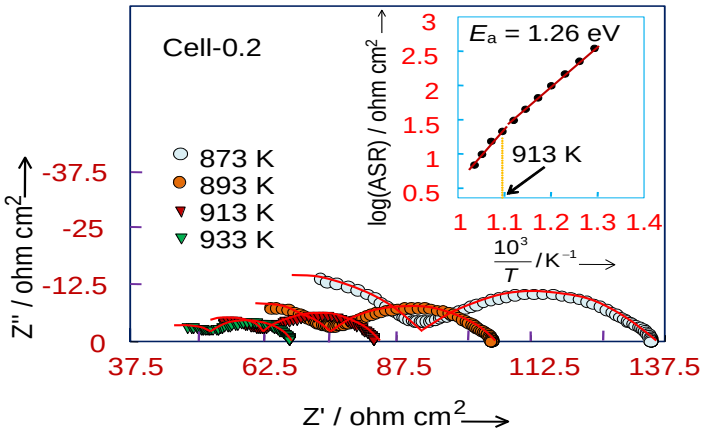

Figure.4. Complex impedance plots for Cell-0.2 at various temperatures experimental data (symbols/points), simulated data (red line); inset shows variation of ASR.

The comparison in Table 3 shows, smallest ASR value obtained in this study with those other K_2NiF_4-typed cathode as reported in literature. Evidently, the ASR of $Nd_{1.8}Sr_{0.2}FeO_{4+\delta}$ in present study is lowest as compared to similar other reported. This lowest value of ASR is may be due to fine microstructure with moderate porosity as well as excellent matching interface between NSFO electrode and CGO electrolyte when the cell is fired at 1273 K [21]. The average size of particle was 1 µm, and the average thickness of the electrode over CGO electrolyte was 14.5 µm (as shown in Fig. 2). Such microstructure facilitates the improved cathode properties [15,21].

Table 3. A comparison of optimum ASR value obtained in this study with values reported in the literature for K_2NiF_4-type cathode.

S. N.	Cathode	ASR (Ω cm^2)	Electrolyte	T (K)	Ref.
1	$Nd_{1.8}Sr_{0.2}NiO_{4+\delta}$	0.52	GDC	973	[31]
2	$La_{1.0}Sr_{1.0}FeO_{4+\delta}$	3.90	SCO	973	[15]
3	$Ba_{1.0}Sr_{1.0}FeO_{4+\delta}$	1.42	LSGM	1073	[36]
4	$Nd_{1.0}Sr_{1.0}FeO_{4+\delta}$	2.75	SDC	973	[21]
5	$Nd_{1.8}Sr_{0.2}FeO_{4+\delta}$	1.92	GDC	973	Present study

The study of area specific resistance under the influence of oxygen partial pressure is useful in determining reaction rate limiting factor over the cathode surface during ORR. The variation between log (R_p) and log(P_{O_2}) at 700 °C is shown in the Fig. 4. Generally, variation in ASR with the reduced oxygen environment follows the below equation;

$$ASR = (ASR)_0 \left(P_{O_2}\right)^{-n} \tag{2}$$

The important information about the limiting factor present in oxygen reduction reactions at cathode surface is obtained from the value of *n* [32,33].

$n = 1$; $O_2(g) \leftrightarrow O_2(ads)$ (3)

$n = 0.5$; $O_2(ads) \leftrightarrow 2O(ads)$ (4)

$n = 0.25$; $O_{(ads)} + 2e^{'} + V_O^{\bullet\bullet} \Leftrightarrow O_O^x$ (5)

$n = 0.1$; $O_{TPB}^{2-} + V_O^{\bullet\bullet} \Leftrightarrow O_O^x$ (6)

The estimated value of *n* (= 0.249 at 923 K) is close to 0.25 for Cell-0.2 (inset of Fig. 5). Fig. 5 suggests that, *n* value increases as the temperature is increased. Same results are obtained for Ln_2MO_4 (M = Ni/Fe) [15,18]. This may be due to, at large temperature (973 K), the transfer of ionic oxygen is improved appreciably in both the electrode and electrode–electrolyte interface. Similar reports are presented by Sun et al. for $Nd_{1.6}Sr_{0.4}NiO_{4+\delta}$ [34]. The study from P_{O_2} measurements concludes that, the charge-transfer at electrode and electrolyte interface is the limiting factor while oxygen reduction reaction. Various research groups have analysed and obtained similar P_{O_2} -reliant ASR nature in MIECs, based on the Eqs. 3-6 [12,35].

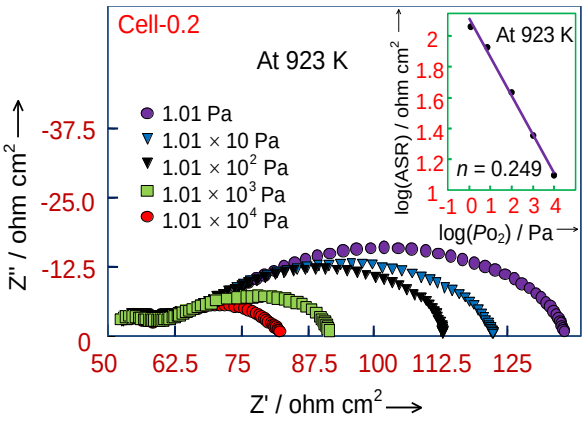

Figure 5. Complex impedance plots of Cell-0.2 for different oxygen partial pressure; inset shows variation of ASR with oxygen partial pressure at 923 K.

4. Conclusions

The series of $Nd_{2-x}Sr_xFeO_{4+\delta}$ (x = 0.1 - 0.4) single phase solid solutions is prepared with crystallite size in submicron range using combustion synthesis technique. XRD backs up tetragonal symmetry (I_4/mmm) of $Nd_{1.8}Sr_{0.2}FeO_{4+\delta}$. The Nd_2FeO_4 lattice increases along the c-axis with Sr content. The agglomeration of the submicron sized crystallites resulted into formation of porous electrode layer is realized from scanning electron microscopy. The dc conductivity results showed maximum σ for x = 0.2, which also exhibited minimum activation energy. The smallest dc conductivity for $x = 0.2$ is due to high porosity as obtained from agglomerated submicron crystallites. The complex impedance plots of the symmetric cell showed decrease in the real axis intercept with increased temperature in turn reduced area specific resistance (ASR). $Nd_{1.8}Sr_{0.2}FeO_{4+\delta}$ cathode exhibits lowest ASR (= 1.92±0.015 Ohm cm^2) at 973 K. The oxygen partial pressure dependent ASR indicated charge transfer at electrode-electrolyte interface is the rate limiting factor while oxygen reduction reaction (ORR).

Above findings, $Nd_{1.8}Sr_{0.2}FeO_{4+\delta}$ could be a promising candidate of cathode material for intermediate temperature solid oxide fuel cell applications.

Acknowledgments

The authors are thankful to Department of Physics, RTM Nagpur University and SAIF, IIT Bombay, Powai, Mumbai for making available characterization facility.

References

[1] Skinner SJ, and Kilner JA. 2000 Solid State Ionics **135** 709.
[2] Boehm E, Bassat JM, Dordor P, Mauvy F, Grenier JC, and Stevens P 2005 Solid State Ionics **176** 2717.
[3] M. L. Fontaine, C. Laberty-Robert, M. Verelst, J. Pielaszeck, P. Lenormand, F. Ansart, and P. Tailhades, 2006 Material Research Bulletin **41** 1747.
[4] Li Q, Zhao H, and Huo LH 2007 Electrochemistry Communications **9** 1508.
[5] Ghorbani-Moghadam T, Kompany A, and Bagheri-Mohagheghi MM, 2018 Ceram Int. **44** 21238.
[6] Garali M, Kahlaoui M, and Mohammed B, 2019 Int J Hydrogen Energy, **44** 11020.
[7] Sandoval MV, Pirovano C, and Capoen E, 2017 Int J Hydrogen Energ, **42** 21930.
[8] M. A. Daraukh, V. V. Vashook, H. Ullmann, F. Tietz, I, and Arual Raj, 2003 Solid State Ionics, **158** 141.
[9] Solak N, Zinkevich M, and Aldinger F 2006 Solid State Ionics, **177** 2139.
[10] Fontaine ML, Laberty-Robert C, Ansart F, and Tailhades P 2006 J Power Sources, **156** 33.
[11] Vashook V, Zosel J, Wen TL, Guth U 2006 Solid State Ionics, **177** 1827.

[12] Mauvy F, Bassat JM, Boehm E, Manaud JP, Dordor P, and Grenier JC 2003 Solid State Ionics **158** 17.
[13] Lalanne C, Mauvy F, Siebert E, Fontaine ML, Bassat JM, Ansart F, Stevens P, and Grenier JC 2007 J Eur Ceram Soc **27** 4195.
[14] Chaudhari VN, Khandale AP, and Bhoga SS 2014 J Power Sources, **248** 647.
[15] Huang J, Jiang X, and Li X, A. Liu, 2009 J Electroceram. **23** 67.
[16] Vashook VV, Trofimenko NE, Ullmann H, Makhnach LV, 2000 Solid State Ionics **131** 329.
[17] Vashook VV, Yushkeivich II, Kokhonovsky LV, Makhonovsky LV, Makhanch LV, Tolochko SP, Kononyuk IF, Ullmann H, Altenburg H, 1999 Solid State Ionics **119** 23.
[18] Vashook VV, Tolochko SP, Yushkeivich II, Makhanch LV, Kononyuk IF, Altenburg H, Hauck J, and Ullmann H, 1998 Solid State Ionics **110** 245.
[19] Ishikawa K, Kondo S, Okanc H, Suzuki S, and Suzuki Y, 2006 Bull. Chem. Soc. Jpn. **60** 1174.
[20] Jin C, Liu J, Zhang YH, Sui J, and Guo WM 2008 J Power Sources **182** 482.
[21] Guo W, Liang H, Pei J, Jin C, and Liu J, 2012 J Solid State Electrochem **16** 83.
[22] Khandale AP, and Bhoga SS, 2012 J. Solid State Electrochem. **16** 341.
[23] Jin C, and Liu J. 2009 J Alloys Compd **474** 573.
[24] Lou X, Liu Z, Wang S, Xiu Y, Wong CP, and Liu M. 2010 J Power Sources **195** 416.
[25] Goodenough JB, and Manthiram A. 1990 J Solid State Chem, **88** 115.
[26] Nakamura T, Yashiro K, Sato K, and Mizusaki J, 2010 Solid State Ionics **181** 292.
[27] Vashook VV, Yushkeivich II, Kokhonovsky LV, Makhonovsky LV, Makhanch LV, Tolochko SP, Kononyuk IF, Ullmann H, and Altenburg H, 1999 Solid State Ionics **119** 23.
[28] Yang J, Cheng J, Jiang Q, Wang Y, Wang R, and Gao J, 2012 Int. J. Hydrogen Energy **37** 1746.
[29] Petrov AN, Zuev AY, and Degtyarev MA, 1998 J. Inorg. Chem. Rus. **72** 44.
[30] Vashook VV, Girdauskaite E, Zosel J, Wen TL, Ullmann H, and Guth U, 2006 Solid State Ionics **177** 1163.
[31] Khandale AP, Punde JD, and Bhoga SS, 2013 Solid State Electrochem **17** 617.
[32] Sicbeit E, Hammouche A, and Kleitz M, 1995 Electrochim. Acta **40** 1741.
[33] Kim JD, Kim GD, Moon JW, Park Y, Lee WH, Kobayashi K, Nagai M, and Kim CE, 2001 Solid State Ionics **143** 379.
[34] Sun Li-P, Li Q, Zhao H, Huo LH, and Grenier JC, 2008 Journal of Power Sources **183** 43.
[35] Aguadero A, Alonso JA, Escudero MJ, and Daza L, 2008 Solid State Ionics **179** (11–12) 393.